New Journal of Physics
The open-access journal for physics

Ultra-cold ion–atom collisions: near resonant charge exchange

E Bodo[1,3], P Zhang[2] and A Dalgarno[2]

[1] Department of Chemistry, University of Rome 'Sapienza', P.le A Moro 5, 00185, Rome, Italy

[2] Institute for Theoretical Atomic and Molecular Physics (ITAMP), Harvard-Smithsonian Center for Astrophysics, Cambridge, MA, USA

E-mail: bodo@caspur.it

New Journal of Physics **10** (2008) 033024 (9pp)
Received 13 November 2007
Published 17 March 2008
Online at http://www.njp.org/
doi:10.1088/1367-2630/10/3/033024

Abstract. Accurate calculations of the near resonant charge exchange cross-sections in HD^+, HT^+ and DT^+ at very low energies are presented. The charge exchange process between an ion and its parent atom is a near resonant process that becomes inelastic when two different isotopes are involved. We find that, at very low energies, the charge exchange cross-section follows Wigner's law for inelastic processes and becomes much larger than the cross-section for elastic collisions which tends to a finite limit. The efficiency of inelastic charge exchange increases as the mass difference between the two isotopes decreases.

Contents

[3] Author to whom any correspondence should be addressed.

© IOP Publishing Ltd and Deutsche Physikalische Gesellschaft

1. Introduction

The possibility of creating small ensembles of ultracold atoms and molecules has opened a new research in atomic, molecular and optical physics [1]–[3]. These include applications in condensed-matter physics [4], in the measurement of fundamental constants [5], in quantum computing [6, 7] and in ultracold chemistry [8, 9]. One open question lies in the role of electrical charges in ultracold systems [10, 11]. Two decades ago, in studies of atomic ions embedded in liquid helium, the measurement of ion mobilities helped to elucidate the microscopic structure of quantum liquids and served as a valuable probe of their properties. Recent experiments have been directed to observing ultracold atomic systems in which electric charges may play an analogous role: these include ultracold plasmas [12], ultracold Rydberg gases [13, 14] and direct ionization experiments in BEC [15, 16]. Observations of atomic and molecular collision processes involving ions at low energies can also be performed using Coulomb crystals [17], where an array of trapped atomic ions or sympathetically cooled molecular ions [18] is used as a cold target buffer because of its spatial localization and the low translational temperatures of 10 mK.

In the collision of a positive ion with its parent atom of the same isotopic composition the identity of the nuclei must be taken into account and charge transfer collisions

$$\mathrm{A} + \mathrm{A}^+ \rightarrow \mathrm{A}^+ + \mathrm{A} \tag{1}$$

cannot be distinguished in principle from elastic collisions

$$\mathrm{A} + \mathrm{A}^+ \rightarrow \mathrm{A} + \mathrm{A}^+. \tag{2}$$

At high collision velocities, an empirical distinction is possible. The angular differential scattering cross-section has two peaks, one in the forward direction which may be attributed to elastic collisions and the other in the backward direction which may be attributed to charge transfer collisions. The corresponding total cross-sections tend in the limit of zero kinetic energy to finite values. The cross-sections are determined theoretically by the interaction potentials of the gerade and ungerade symmetry states of the molecular ions A_2^+. An explicit example is the calculation for $\mathrm{Na} + \mathrm{Na}^+$ [19].

If different isotopes are involved, there occurs a change in the kinetic energies of the particles in the charge transfer collisions and not in the elastic collisions. The molecular u–g symmetry is broken and the molecular states separate at large internuclear distances to asymptotic binding energies for $\mathrm{A} + \mathrm{A}'^+$ and for $\mathrm{A}^+ + \mathrm{A}'$, differing by a small amount of ΔE that depends on the masses. The Born–Oppenheimer (BO) approximation fails because its symmetry properties are determined by the electronic Hamiltonian. Several theoretical methods have been proposed [20]–[22] in which the BO approximate eigenfunctions are replaced by adiabatic eigenfunctions which incorporate some aspects of the nuclear–electronic coupling and which are constructed so that the colliding species separate asymptotically to the correct limits. Numerical cross-sections have been obtained for the reaction

$$\mathrm{H} + \mathrm{D}^+ \rightarrow \mathrm{H}^+ + \mathrm{D}, \tag{3}$$

and its reverse for kinetic energies down to 10^{-5} eV. We adopt the approach of Hunter *et al* [20] and apply it to reactions involving hydrogen, deuterium and tritium ions and their parent atoms. We carry out calculations of the cross-sections at low energies and determine the complex scattering lengths.

2. Methodology

In the BO approximation the three molecules H_2^+, D_2^+ and HD^+ can all be described using the same $^2\Sigma_{g,u}$ potentials with a dissociation limit of $-1/2$ au. For our purposes a two-state approximation suffices and therefore we do not consider the excited states with higher dissociation limits. When the different mass of the isotopes is correctly considered, the homonuclear symmetry in HD^+ is broken and the two Σ states correlate asymptotically to the exact energies of the isolated neutral atoms in the following way:

$$H + D^+ \rightarrow \quad E_0 = -\mu_H/2, \tag{4}$$

$$H^+ + D \rightarrow \quad E_1 = -\mu_D/2, \tag{5}$$

where μ_H and μ_D are the reduced masses of the hydrogen and deuterium atoms, respectively. The ground state of HD^+ separates to the heavier neutral D atom. We will show that at ultra-low energies the inelastic collision process (charge exchange) that brings the system from $H + D^+$ to the ground state follows Wigner's law and that therefore, at sufficiently low energies, its cross-section becomes infinite.

Hunter *et al* [20] considered the electronic adiabatic solutions of a system composed of two nuclei with masses m_1, m_2 and one electron with mass m_3. After the separation of the center of mass, the Hamiltonian, in au, reads:

$$\left[-\frac{1}{2\mu_1}\nabla_a^2 - \frac{1}{2\mu_2}\nabla_b^2 + V(\mathbf{R}_a, \mathbf{R}_b)\right]\Psi_I = E\Psi_I, \tag{6}$$

where Ψ_I is a function of internal coordinates, $\mu_1 = m_1 m_2/(m_1 + m_2)$ and $\mu_2 = m_3(m_1 + m_2)/(m_1 + m_2 + m_3)$, $\mathbf{R}_a$ is the vector joining the two nuclei and $\mathbf{R}_b$ is the vector joining the nuclear center of mass and the electron. The total wavefunction Ψ_I is expanded in adiabatic states

$$\Psi_I = \sum_i \psi_a^{(i)}(\mathbf{R}_a)\psi_s^{(i)}(R, \mathbf{R}_c), \tag{7}$$

where each of the ψ_s satisfies an electronic equation [20]

$$\left[-\frac{1}{2\mu_2}\nabla_c^2 + V(R, \mathbf{R}_c)\right]\Psi_s(R, \mathbf{R}_c) = E_s(R)\Psi_s(R, \mathbf{R}_c) \tag{8}$$

with $R = |\mathbf{R}_a|$ and $\mathbf{R}_c$ is the vector $\mathbf{R}_b$ after a frame transformation. Equation (8) for the electronic motion is solved by writing $\mathbf{R}_c$ in spheroidal coordinates [20]. Finally, one obtains a set of coupled equations for the nuclear motion in the R coordinate

$$\mathbf{H}\psi_a(R) = \mathbf{E}\psi_a(R). \tag{9}$$

We can write the equation for the nuclear motion at energy $E = k^2/2\mu_{HD}$ in the 2×2 matrix form

$$\left[\mathbf{I}\frac{d^2}{dR^2} - \mathbf{F}\frac{d}{dR} + \mathbf{k^2} - \left(2\mu_{HD}\mathbf{V} + \frac{\mathbf{L^2}}{R^2}\right)\right]\psi_a(R) = 0, \tag{10}$$

where $\mathbf{I}$ is the identity matrix, $\mathbf{L^2}$ and $\mathbf{k^2}$ are diagonal matrices with elements $l(l+1)$ and k_0^2 and k_1^2, where l is the nuclear angular momentum quantum number. The initial and final wavenumbers k_0 and k_1 are related by

$$k_1^2 - k_0^2 = 2\mu_{HD}(E_0 - E_1) = 2\mu_{HD}\Delta E. \tag{11}$$

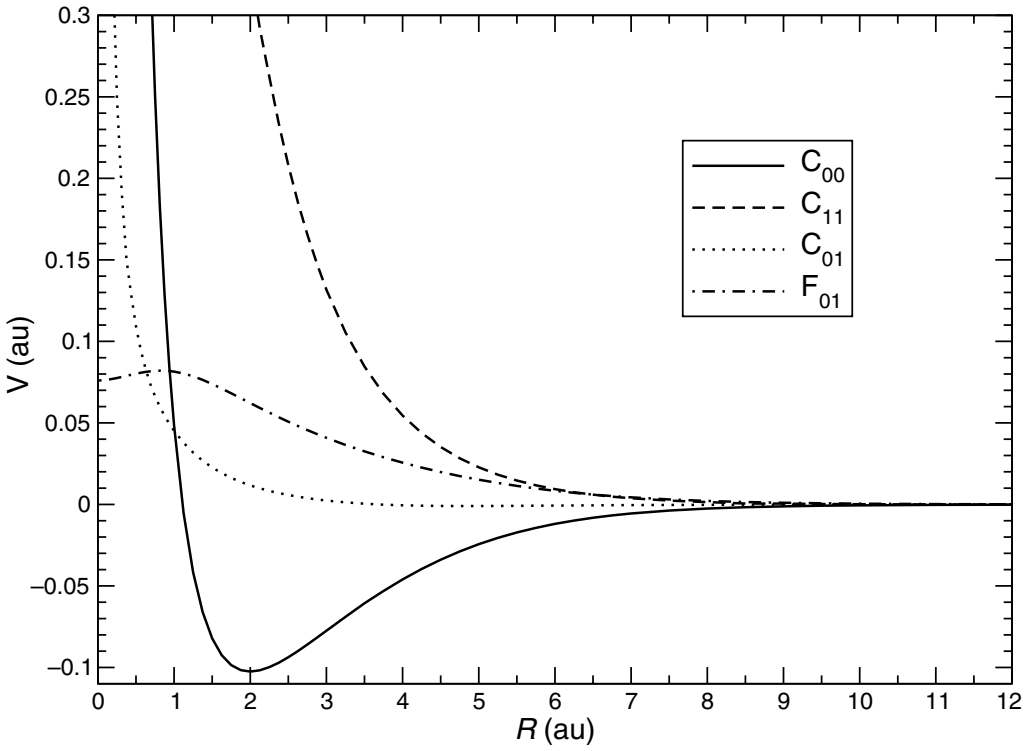

Figure 1. Potentials and coupling strength reconstructed from the data in [20]. The potentials as well as the distance are in au. C_{01} and F_{01} are multiplied by 10^5 to make them visible on the same scale.

The potential matrix elements are given by

$$\begin{aligned} V_{00} &= \tfrac{1}{2}(C_{00}+C_{11})+C_{01}, \\ V_{11} &= \tfrac{1}{2}(C_{00}+C_{11})-C_{01}, \\ V_{01} &= \tfrac{1}{2}(C_{00}-C_{11})-\frac{1}{2}\frac{\mathrm{d}F_{01}}{\mathrm{d}R}, \\ V_{10} &= \tfrac{1}{2}(C_{00}-C_{11})+\frac{1}{2}\frac{\mathrm{d}F_{01}}{\mathrm{d}R}, \end{aligned} \tag{12}$$

where the adiabatic potentials C_{ij} and coupling strength F_{ij} are given in [20] in terms of electronic matrix elements. The C_{ij} and F_{ij} potentials are reported in figure 1.

Solutions to equation (10) and the corresponding cross-sections were found through a modified Numerov algorithm that accounts for the presence of the linear derivative (see appendix) [23]–[25].

3. Results and discussion

We have performed calculations for collision energies from 10^{-9} to 10^{-3} eV above threshold. Convergence has been carefully checked for the integration range, step-size and number of

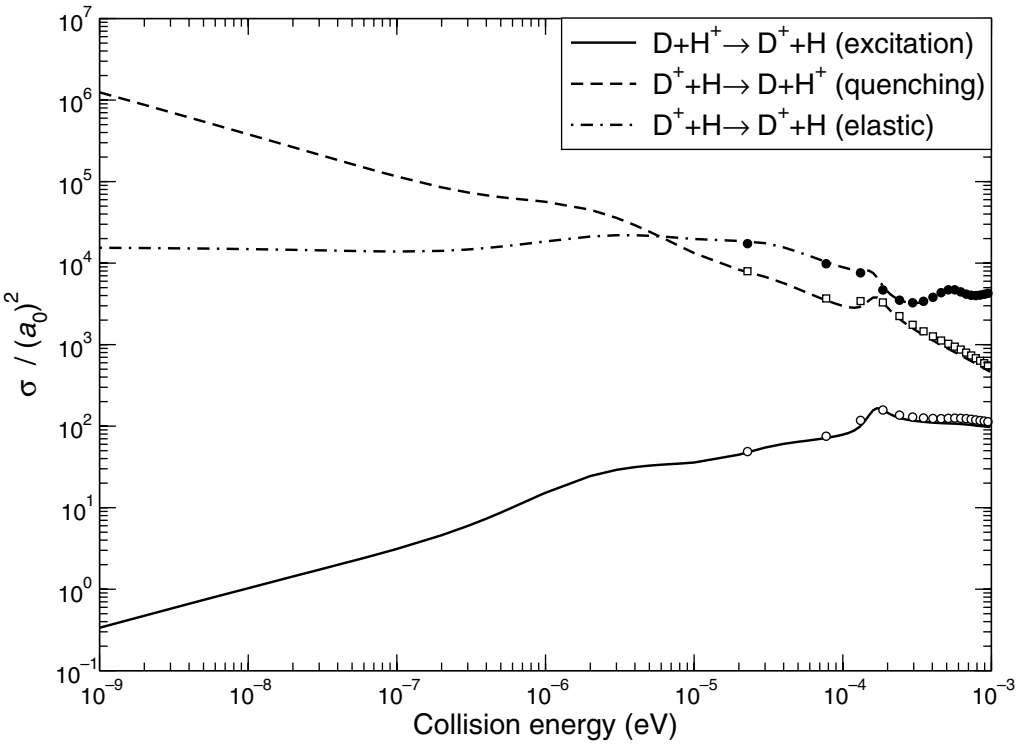

Figure 2. Charge exchange and elastic cross-sections for HD^+ as functions of collision energy above threshold. The symbols are the calculations from [26].

partial waves. We present the cross-sections in figure 2 together with the results of Esry *et al* [26] which refer to collision energies above 3×10^{-5} eV and which were obtained by a different procedure. The close agreement confirms the accuracy of both sets of calculations.
The cross-section labeled 'quenching' which refers to the inelastic exothermic process:

$$D^+ + H \rightarrow D + H^+$$

follows Wigner's law below 10^{-6} eV, the elastic cross-section becomes a constant and the excitation cross-section tends to zero. At ultra-low energies the scattering in the electronically excited state (correlating with $D^+ + H$) can be characterized by a complex scattering length $a = \alpha - i\beta$. We have extracted it from the S matrix at the lowest energy and their values are reported in the first row of table 1. The value of β yields a limiting rate constant at zero Kelvin of $1.9 \times 10^{-9}\,\mathrm{cm^3 s^{-1}}$. This is remarkably large for a weakly exothermic process triggered by extremely small non-adiabatic couplings. As can be seen in figure 2, for energies below 5×10^{-6} eV (~0.5 K) the inelastic process is dominant over the elastic scattering. The reverse inelastic reactions have rate coefficients reduced by the factor $\exp(-\Delta E/kT)$. It is clear from these results that if an ensemble of polarized D and H atoms at ultra-low energies is ionized, the charge will tend rapidly to migrate to the H nuclei leaving the D atoms neutral.

In such an ensemble, however, there exist two other mechanisms for the migration of the charge involving the resonant charge exchange in H_2^+ and D_2^+. In figure 3, we compare the cross-sections for the charge exchange (left panel) and for the elastic process (right panel) for H_2^+, D_2^+ and HD^+. Only in the case of DH^+ we do have an inelastic process during charge exchange and its cross-section is the one that diverges below 10^{-7} eV. It is interesting to note that, for

Table 1. Scattering lengths (in au) for the scattering processes described in the present work. The number next to β is the limiting value at zero Kelvin for the rate constant in $cm^3\ s^{-1}$.

System	α(El)	β/rate($T=0$)
$D^+ + H \rightarrow D + H^+$	15.3	$30.6/1.9 \times 10^{-9}$
$T^+ + H \rightarrow T + H^+$	9.8	$14.5/8.0 \times 10^{-10}$
$T^+ + D \rightarrow T + D^+$	245.9	$451.9/1.6 \times 10^{-8}$
System	$a(\Sigma_g)$	$a(\Sigma_u)$
$H^+ + H \rightarrow H + H^+$	−28.8	+725.2
	−29.3[a]	+750[a]
$D^+ + D \rightarrow D + D^+$	+485.7	−95.6

[a] From [27].

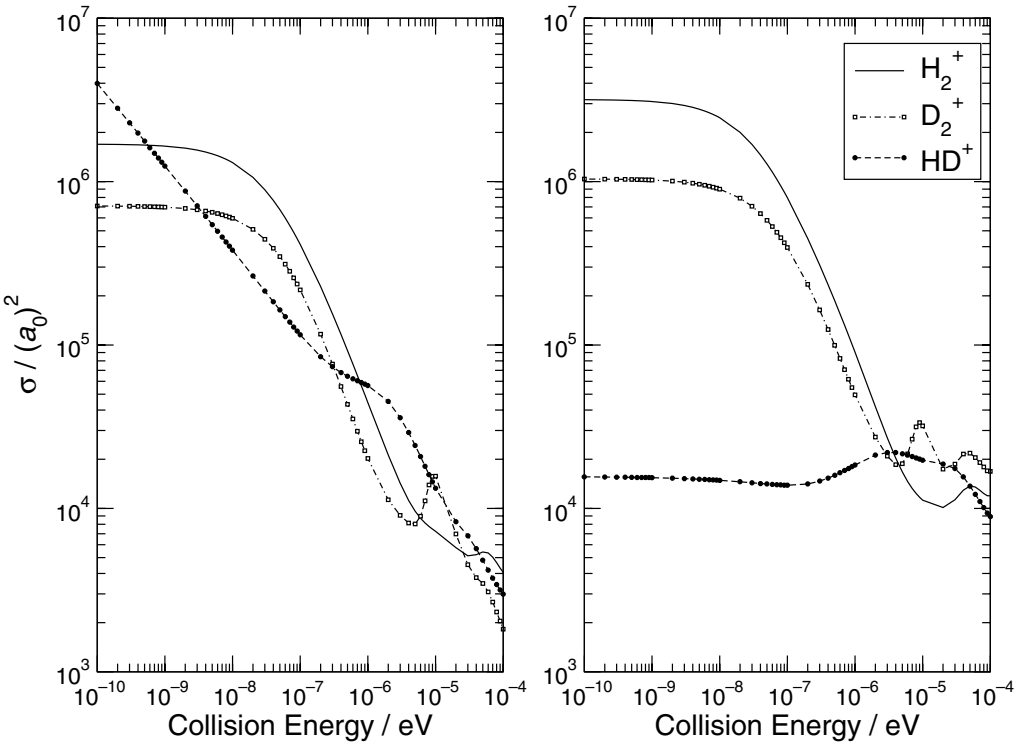

Figure 3. Cross-sections for charge exchange (left) and elastic collisions (right).

the latter system below 10^{-9} eV, the inelastic charge transfer process is more efficient than the elastic one.

In the case of resonant charge transfer β is zero and the scattering is characterized by two real scattering lengths; one for the Σ_g state and the other for the Σ_u state. These data are presented in table 1. The cross-section for elastic collisions is the average of Σ_g and Σ_u cross-sections. The large cross-section found for DT^+ indicates the approach of a zero energy resonance state as the reduced mass increases.

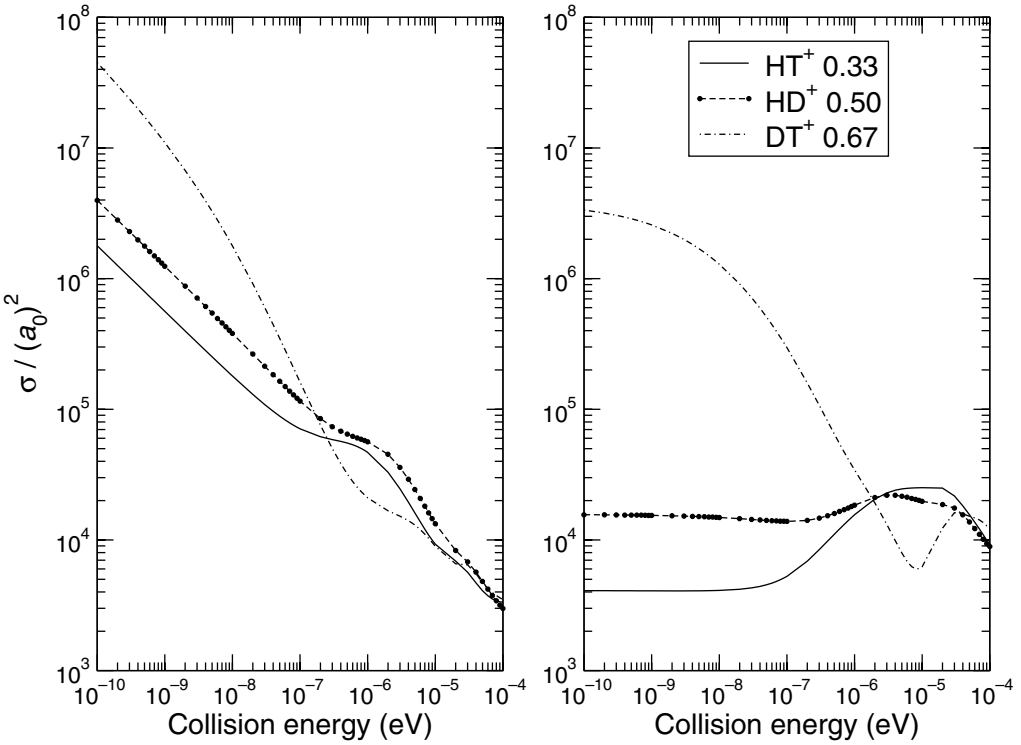

Figure 4. Cross-sections for charge exchange (left) and elastic collisions (right). The numbers in the legend are the mass ratios between the two isotopes involved.

To explore the sensitivity of the cross-sections to the mass and energy differences, we report in figure 4 the cross-sections for the HD^+, HT^+ and DT^+ systems. As the reduced mass increases, the energy difference ΔE between the states decreases from 39.7 cm^{-1} for HT^+, to 29.8 for HD^+, to 9.9 for DT^+. At the same time the inelastic process becomes more efficient in transferring the charge. The huge value of the rate constant that we obtain for the charge exchange in DT^+ of 1.6×10^{-8} cm^3 s^{-1} is a value more typical of ionic reactions than that of a process which is mainly triggered by the non-adiabatic effects that arise from the small electron–nuclei motion couplings.

4. Conclusions

We have analyzed the general problem of ultracold collisions between an ion and an atom corresponding to two different isotopes. The charge exchange process is inelastic, the BO approximation breaks down and the process is driven by the weak coupling of the nuclear and electronic motion. In contrast to ion–atom collisions involving one isotope for which the cross-section is finite at zero energy, the cross-section for the exoergic charge exchange process tends to infinity as the inverse of velocity in accordance with Wigner's law. We have shown that if the energy difference is small the charge exchange rate is very fast. We conclude that in a gas with a mixture of isotopes the charge will migrate to the heavier isotope with high efficiency.

Acknowledgments

We are grateful to Dr H R Sadeghpour for providing us with the numerical values of the cross-sections reported in [26]. This research was partly supported by the Chemical Sciences, Geosciences and Biosciences Division of the Office of Basic Energy Science, Office of Science, US Department of Energy and partly by the NSF through the Harvard-MIT Center for Ultracold Atoms (AD and PZ). EB acknowledges travel support from the Institute for Theoretical Atomic, Molecular and Optical Physics which is funded by the NSF.

Appendix. Generalized Numerov propagator

Our nuclear problem is given by:

$$\left[\frac{\mathrm{d}^2}{\mathrm{d}R^2}\mathbf{I} - \mathbf{F}\frac{\mathrm{d}}{\mathrm{d}R} + \mathbf{k^2} - \left(2\mu_{\mathrm{HD}}\mathbf{V} + \frac{\mathbf{L^2}}{R^2}\right)\right]\boldsymbol{\Psi}(R) = 0. \tag{A.1}$$

By setting

$$\mathbf{Q}(x) = \mathbf{k^2} - \left(2\mu_{\mathrm{HD}}\mathbf{V} + \frac{\mathbf{L^2}}{R^2}\right) \quad \text{and} \quad \mathbf{P}(x) = -\mathbf{F}, \tag{A.2}$$

equation (A.1) can be written as

$$\left[\mathbf{I}\frac{\mathrm{d}^2}{\mathrm{d}R^2} + \mathbf{P}(x)\frac{\mathrm{d}}{\mathrm{d}R} + \mathbf{Q}(x)\right]\boldsymbol{\Psi}(x) = 0. \tag{A.3}$$

The extended Numerov method we have implemented is very similar to the multichannel Numerov propagator of Johnson [23] and is based on the following two terms recursion relation for the **R** matrix

$$\mathbf{R}_n = \mathbf{U}_n\mathbf{Y}_n^{-1} - \mathbf{Z}_n\mathbf{Y}_n^{-1}\mathbf{R}_{n-1}^{-1}, \tag{A.4}$$

where

$$\begin{aligned}
\mathbf{U}_n &= (2 + 10\mathbf{T}_n)\boldsymbol{\alpha}_n - 2h^2\mathbf{P}^{\dagger}(x_n)\mathbf{P}(x_n)\mathbf{T}_n,\\
\mathbf{Y}_n &= \boldsymbol{\alpha}_n - h\mathbf{P}(x_n)(\tfrac{1}{2} - \mathbf{T}_{n+1})(1 - \mathbf{T}_{n+1})^{-1},\\
\mathbf{Z}_n &= \boldsymbol{\alpha}_n + h\mathbf{P}(x_n)(\tfrac{1}{2} - \mathbf{T}_{n-1})(1 - \mathbf{T}_{n-1})^{-1},
\end{aligned} \tag{A.5}$$

where $\boldsymbol{\alpha} = 1 + h^2/6(\mathbf{P}'(x_n) + \mathbf{P}^{\dagger}(x_n)\mathbf{P}(x_n))$ and $\mathbf{T}_n = -h^2/12\mathbf{Q}(x_n)$. It is possible to obtain $\boldsymbol{\Psi}$ from **R** at each point by using

$$\boldsymbol{\Psi}_{n+1} = (1 - \mathbf{T}_{n+1})^{-1}\mathbf{R}_n(1 - \mathbf{T}_n)\boldsymbol{\Psi}_n. \tag{A.6}$$

The inner boundary condition is obtained by letting $\mathbf{R}(x_1)$, with x_1 well inside the classical forbidden region, be a diagonal matrix set to a very large number. Equation (A.4) is then used throughout the integration range up to x_N which is sufficiently far out in the asymptotic region. The matching condition is done through equations (A.16)–(A.19) of [23] and from it we get the S matrix.

The propagation is repeated for each contributing value of the angular momentum l and the S matrix is then used in the familiar way in order to obtain the charge exchange cross-section:

$$\sigma_{\mathrm{ct}}(i \to j) = \frac{\pi}{k_i^2} \sum_l (2l+1)|S_{ij}^l|^2 \tag{A.7}$$

and the elastic cross-section

$$\sigma_{\mathrm{el}}(i \to i) = \frac{\pi}{k_i^2} \sum_l (2l+1)|1 - S_{ii}^l|^2. \tag{A.8}$$

References

[1] Bethlem H L and Meijer G 2003 *Int. Rev. Phys. Chem.* **22** 73
[2] Doyle J, Friedrich B, Krems R V and Masnou-Seeuws F 2004 *Eur. Phys. J.* D **31** 149
[3] Krems R V 2005 *Int. Rev. Phys. Chem.* **24** 99
[4] Jochim S, Bartenstein M, Altmeyer A, Hendl G, Riedl S, Chin C, Hecker J, Denschtag J and Grimm R 2003 *Science* **302** 2101
[5] Fortson N, Sandars P and Barr S 2003 *Phys. Today* **56** 33
[6] André A, DeMille D, Doyle J M, Lukin M D, Maxwell S E, Rabl P, Schoelkopf R J and Zoller P 2006 *Nat. Phys.* **2** 636
[7] Micheli A, Brennen G K and Zoller P 2006 *Nat. Phys.* **2** 341
[8] Balakrishnan N and Dalgarno A 2001 *Chem. Phys. Lett.* **341** 652
[9] Bodo E, Gianturco F A, Balakrishnan N and Dalgarno A 2004 *J. Phys. B: At. Mol. Opt. Phys.* **37** 3641
[10] Côté R 2000 *Phys. Rev. Lett.* **85** 5316
[11] Côté R, Kharchenko V and Lukin M D 2002 *Phys. Rev. Lett.* **89** 093001
[12] Killian T C, Kulin S, Bergeson S D, Orozco L A, Orzel C and Rolston S L 1999 *Phys. Rev. Lett.* **83** 4776
[13] Anderson W R, Veale J R and Gallagher T F 1998 *Phys. Rev. Lett.* **80** 249
[14] Mourachko I, Comparat D, De Tomasi F, Fioretti A, Nosbaum P, Akulin V M and Pillet P 1998 *Phys. Rev. Lett.* **80** 253
[15] Kraft S, Günther A, Fortágh J and Zimmermann C 2007 *Phys. Rev.* A **75** 063605
[16] Massignan P, Pethick C J and Smith H 2005 *Phys. Rev.* A **71** 033607
[17] Drewsen M, Jensen I, Lindballe J, Nissen N, Martinussen R, Mortensen A, Staanum P and Voigt D 2003 *Int. J. Mass Spectrom. Ion Process.* **229** 83
[18] Jorgensen S, Drewsen M and Kosloff R 2005 *J. Chem. Phys.* **123** 094302
[19] Côté R and Dalgarno A 2000 *Phys. Rev.* A **62** 012709
[20] Hunter G, Gray B F and Pritchard H O 1966 *J. Chem. Phys.* **45** 3806
[21] Igarashi A and Lin C D 1999 *Phys. Rev. Lett.* **83** 4041
[22] Esry B D and Sadeghpour H R 1999 *Phys. Rev.* A **60** 3604
[23] Johnson B R 1978 *J. Chem. Phys.* **69** 4678
[24] Leroy J P and Wallace R 1985 *J. Phys. Chem.* **89** 1928
[25] Tselyaev V 2004 *J. Comp. Appl. Math.* **170** 103
[26] Esry B D, Sadeghpour H R, Wells E and Ben-Itzhak I 2000 *J. Phys. B: At. Mol. Opt. Phys.* **33** 5329
[27] Carbonell J, Lazauskas R, Delande D, Hilico L and Kiliç S 2003 *Europhys. Lett.* **64** 316